Wannier-like equation for the resonant cavity modes of locally perturbed photonic crystals

Oskar Painter,* Kartik Srinivasan, and Paul E. Barclay
Department of Applied Physics, California Institute of Technology, Pasadena, California 91125, USA
(Received 17 February 2003; revised manuscript received 2 June 2003; published 30 July 2003)

In analogy to the Wannier equation for localized electronic impurity states in crystalline materials, a wave equation for the envelope of the resonant optical modes of local defects within two-dimensional periodic dielectric structures is derived. In the case of degenerate satellite extrema, this is generalized to a set of coupled Wannier-like equations for a multienvelope system. The localized Wannier envelope solutions are then used in conjunction with a group theoretical symmetry analysis to determine an approximate form for donor and acceptor modes in a hexagonal photonic crystal. For an effective harmonic potential formed by varying the filling fraction of the lattice, the localized resonant modes are explicitly calculated using the Wannier equation and symmetry analysis, and a comparison to exact numerically computed modes is presented.

DOI: 10.1103/PhysRevB.68.035214 PACS number(s): 42.70.Qs, 42.55.Sa, 42.60.Da, 42.55.Px

I. INTRODUCTION

Beginning with the first proposal of spontaneous emission control[1,2] using three-dimensional photonic band gap materials in 1987 by Yablonovitch,[3] there has been an increasing interest in, and effort towards, applying multi-periodic high-contrast dielectric and metallic structures for the diffraction, guiding, and localization of light in optoelectronic applications. A particularly interesting geometry for such applications is that of planar two-dimensional (2D) photonic crystal (PC) slab waveguide structures,[4–6] where practical fabrication issues are balanced against the extent of the attainable photonic band gap. In such structures, local modifications (defects) of the photonic lattice have been used to form nanometer-scale lasers,[7–10] add-drop filters,[11] and coupled-cavity-waveguide systems.[12–15]

Most of the planar 2D PC structures to date have been analyzed using numerical methods such as the finite-difference time-domain (FDTD) algorithm. These techniques are extremely useful in providing accurate field profiles and frequencies, but are for the most part ineffective in motivating new and interesting device designs. One would hope to develop an approximate model of the properties of nonuniform photonic crystals which depends more transparently upon the dielectric lattice and its band structure. This has been largely accomplished by Russell and Birks,[16,17] where in analogy to the work on Bloch electron dynamics,[18,19] they developed a *semiclassical* picture of ray optics (Hamiltonian optics[20]) within nonuniform photonic crystals to study the propagation of the optical envelope (ray). In this formalism the local band structure is used to arrive at a spatially varying Hamiltonian, and the evolution of the optical envelope in real and reciprocal space is governed by Hamilton's equations in which the conjugate momentum to the (coarse grained) spatial coordinates is taken as the crystal momentum **k**. This method has been used to describe in an elegant and intuitive way the properties of fiber Bragg gratings, 2D PC based wavelength-division multiplexing devices and closed-orbit paths (localized resonances). A systematic formalism, based upon the multiple scales method, has also been developed by Sipe *et al.*[21] and de Sterke *et al.*[22] to generate a rigorous coupled-mode theory for nonuniform (and nonlinear) grating structures. These coupled-mode equations are then used by the authors to describe an effective medium in which the effective fields are the amplitudes (envelopes) of the Bloch waves of the photonic crystal and the imaginary regions of the effective refractive index are related to the local band gap of the nonuniform grating.

In this paper, in analogy to the study of localized impurity states of electrons in periodic crystals,[23–26] we look to develop a Wannier-like *wave equation* to describe the envelope of resonant modes of localized perturbations within periodic dielectric structures. This has been done previously, in a more restrictive setting by Johnson *et al.*[27], and more recently in a general way by Charbonneau-Lefort *et al.*[28] and Istrate *et al.*[29] in the study of photonic crystal heterostructures. In these works, a wave equation for localized modes of nonuniform photonic crystals using an envelope approximation has been developed; however, in each case the envelope equation was formulated as a generalized Hermitian eigenvalue equation in terms of the *electric field*, and more importantly, localized modes formed from nondegenerate satellite extrema were only considered. In the analysis presented here we: (i) consider the magnetic field, and (ii) incorporate the mixing amongst the degenerate peaks or valleys of the orbit of **k** in the band structure, resulting in a set of coupled Wannier-like equations describing a multienvelope system. This allows us to more easily apply the envelope formalism to resonant cavity modes of PC slab waveguides, which in a two- or three-dimensional crystal mix Bloch modes near the degenerate satellite extrema of the orbit of **k**. We also focus on the magnetic field as it can be approximately treated as a scalar for TE-like polarization modes of PC slabs,[39] a technologically important system owing to the large band gap obtainable for modes of this polarization in connected dielectric lattices. From the shape and symmetry of the envelope of a localized resonant mode, and its relation to the underlying photonic band structure, one may better design such features of planar 2D PC resonant cavities as in-plane and vertical emission, resonator-waveguide coupling, and the quality factor of resonant modes. In addition, the Wannier-like equation for localized defect modes, more clearly and rigorously

relates the curvature of the band structure to the formation of donor and acceptor modes for different types of local perturbations of a dielectric lattice.

The paper is organized as follows. In Sec. II we derive a set of coupled Wannier-like equations for the envelope functions of localized TE-like states in planar 2D PC structures, where, as predicted by the Wannier theorem, the underlying band structure of the periodic dielectric structure gives rise to an effective mass tensor. We also derive an approximate form for the effective potential in the Wannier envelope equation in terms of the local perturbation to the dielectric lattice. In Sec. III we calculate an approximate symmetry basis for the TE-like Bloch modes at the valence and conduction band edge of the first-order band gap in a 2D photonic crystal consisting of a hexagonal array of air holes. From this symmetry basis we derive approximate relations for the effective mass tensor of the Wannier equation, and in conjunction with a symmetry analysis used to determine the mixing among the degenerate satellite extrema, we find an approximate form for the localized donor and acceptor modes of a hexagonal lattice with a parabolically graded filling fraction. For comparison, numerical calculations using FDTD of the acceptor and donor modes of such a defect cavity are also presented.

II. WANNIER THEOREM FOR PHOTONS IN PERIODIC DIELECTRIC STRUCTURES

In studying the localized electronic states associated with impurities within a crystalline material it is often helpful to transform Schrödinger's equation into Fourier space, simplify the set of coupled equations through the limited Fourier decomposition of the perturbing potential, and then retransform back to real-space coordinates where a wave equation for the envelope of the localized states is generated. The Wannier theorem[18] captures the essence of this procedure in using the underlying energy-(crystal)momentum dispersion generated by the periodic Coulombic potential of the crystal in a spatially coarse-grained theory of electron dynamics. One application of the Wannier theorem is in the calculation of bound electronic states of crystal impurities.[23–26,30] The basic form of the Wannier equation for the envelope of impurity states is

$$\{[\mathcal{E}-\mathcal{E}_n(\hbar^{-1}\hat{\mathbf{p}})]+\Delta V(\mathbf{r})\}\Gamma(\mathbf{r})=0, \tag{1}$$

where $\mathcal{E}_n(\hbar^{-1}\hat{\mathbf{p}})$ is the energy-(crystal)momentum dispersion relation of the nth energy band with wave vector $\mathbf{k}$ replaced by the canonical momentum operator $\hat{\mathbf{p}}=-i\hbar\nabla$, $\Delta V(\mathbf{r})$ is the impurity potential, and $\Gamma(\mathbf{r})$ is the envelope function describing the localized electronic state.

We would like to find a similar Wannier-like equation for the envelope of localized photon states in periodic dielectric lattices. Of particular interest are the localized resonant modes of planar 2D PCs formed in optically thin dielectric slabs (see Fig. 1). The fundamental TE-like even modes and TM-like odd modes of a symmetric 2D patterned dielectric slab waveguide can be approximated by scalar fields. In what follows we shall focus on the TE-like modes (as discussed in the Appendix a similar theory may also be derived for the

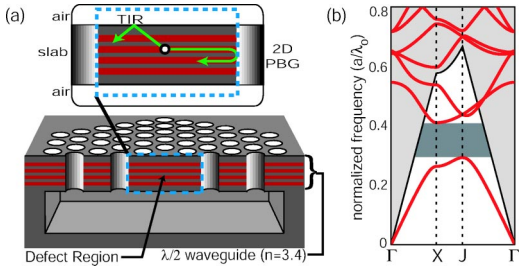

FIG. 1. (a) Illustration of the two-dimensional hexagonal PC slab waveguide structure. (b) Fundamental TE-like (even) guided mode band structure ($r/a=0.36$, $n_{\mathrm{slab}}=n_{\mathrm{eff}}=2.65$). The guided mode band-gap extends over a normalized frequency of 0.29–0.41. The air (cladding) light line is shown as a solid black line.

TM-like modes of the PC slab) as it is for these modes that a significant frequency band gap opens up in the case of connected dielectric lattices such as those used to form laser cavities[10] and optical waveguides.[31] For the fundamental TE-like even modes the magnetic field can be approximated by its $\hat{z}$-component normal to the plane of the slab (only strictly valid in the horizontal mirror plane of a symmetric slab). This reduces the problem to an effective scalar field theory in which $\mathbf{H}(\mathbf{r})\approx\hat{z}H(\mathbf{r}_\perp)$, with $\mathbf{r}_\perp$ labeling the coordinates within the horizontal plane of the slab (to simplify notation, from here on we drop the $\perp$ label from the in-plane coordinates). The scalar field eigenvalue equation for the magnetic field in this quasi-2D approximation is (see the Appendix),

$$\hat{\mathcal{L}}_H^{\mathrm{TE}}H_{\mathrm{d}}=\lambda_{\mathrm{d}}H_{\mathrm{d}}, \tag{2}$$

where $\lambda_{\mathrm{d}}=(\omega_{\mathrm{d}}/c)^2$, ω_{d} is the angular frequency of the defect mode, c the speed of light in vacuum, and

$$\hat{\mathcal{L}}_H^{\mathrm{TE}}=-\nabla(\eta_o+\Delta\eta)\cdot\nabla-(\eta_o+\Delta\eta)\nabla^2. \tag{3}$$

η_o is given by the inverse of the the square of the refractive index of the unperturbed photonic crystal, $1/n_{2D}^2(\mathbf{r})$, and $\Delta\eta$ represents the localized perturbation to $1/n_{2D}^2(\mathbf{r})$. The eigenoperator $\hat{\mathcal{L}}_H$ (we drop the TE superscript from here on) can be separated into an unperturbed photonic crystal part, $\hat{\mathcal{L}}_{H,o}=-\nabla(\eta_o)\cdot\nabla-\eta_o\nabla^2$, and a perturbation part due to the defect, $\hat{\mathcal{L}}'_H=-\nabla(\Delta\eta)\cdot\nabla-\Delta\eta\nabla^2$.

The (2D approximate) modes of the perfect crystal are eigenmodes of $\hat{\mathcal{L}}_{H,o}$,

$$\hat{\mathcal{L}}_{H,o}H_{l,\mathbf{k}}=\lambda_{l,\mathbf{k}}H_{l,\mathbf{k}}, \tag{4}$$

where l labels the band index and $\mathbf{k}$ labels the in-plane crystal momentum. As the $H_{l,\mathbf{k}}$ are Bloch waves they can be written as

$$H_{l,\mathbf{k}}=\frac{1}{L}h_{l,\mathbf{k}}(\mathbf{r})e^{i\mathbf{k}\cdot\mathbf{r}}, \tag{5}$$

with L^2 equal to the area of the 2D photonic crystal and the set of periodic functions, $h_{l,\mathbf{k}}(\mathbf{r})$, at crystal momentum $\mathbf{k}$, satisfying their own set of orthogonality relations (normalized over the lattice unit cell v)

$$\langle h_{l',\mathbf{k}}|h_{l,\mathbf{k}}\rangle_v \equiv \frac{1}{v}\int_v d^2r\, h^*_{l',\mathbf{k}} h_{l,\mathbf{k}} = \delta_{l',l}. \tag{6}$$

In forming a defect state by perturbing the lattice in a localized region of space, the Bloch modes in proximity to the degenerate satellite extrema of a band edge, the $\{\mathbf{k}_i; i=1,2,\ldots,M\}$ points of the $\star\mathbf{k}$ (from here on reference to the $\star\mathbf{k}$ refers implicitly to the orbit of this band edge), are most strongly coupled together:[25]

$$H_{\mathrm{d}}(\mathbf{r}) = \sum_i\ c_i \sum_{\mathbf{k}}\ \tilde{\Gamma}_i(\mathbf{k}-\mathbf{k}_i)\frac{1}{L}h_{l,\mathbf{k}}e^{i\mathbf{k}\cdot\mathbf{r}}. \tag{7}$$

$\tilde{\Gamma}_i$ are a set of Fourier space envelope functions, which, in the spirit of the effective mass theory, have amplitudes localized around $\mathbf{k}=\mathbf{k}_i$. Note that throughout this analysis the band of interest at the band edge is considered to be nondegenerate and we neglect *inter*band mixing.[25]

Assuming that the $h_{l,\mathbf{k}}$ do not vary significantly (using a similar argument as in Ref. 24) over the range of each Fourier space envelope function,

$$H_{\mathrm{d}}(\mathbf{r}) \approx \sum_i\ c_i \frac{1}{L}h_{l,\mathbf{k}_i}e^{i\mathbf{k}_i\cdot\mathbf{r}}\left(\sum_{\Delta\mathbf{k}}\ \tilde{\Gamma}_i(\Delta\mathbf{k})e^{i\Delta\mathbf{k}\cdot\mathbf{r}}\right), \tag{8}$$

where $\Delta\mathbf{k}\equiv\mathbf{k}-\mathbf{k}_i$. Writing the envelope functions in real space,

$$\Gamma_i(\mathbf{r}) = \sum_{\Delta\mathbf{k}}\ \tilde{\Gamma}_i(\Delta\mathbf{k})e^{i\Delta\mathbf{k}\cdot\mathbf{r}}, \tag{9}$$

allows us to rewrite Eq. (8) as

$$H_{\mathrm{d}}(\mathbf{r}) \approx \sum_i\ c_i \frac{1}{L}h_{l,\mathbf{k}_i}e^{i\mathbf{k}_i\cdot\mathbf{r}}\,\Gamma_i(\mathbf{r}). \tag{10}$$

It is in this way that the real space envelope of localized defect modes can be interpreted in the Fourier domain[24] as a result of the *intra*band mixing of the unperturbed Bloch modes of the crystal.

Returning to Eq. (2), we now proceed to find an eigenvalue equation for the envelope functions. Multiplying both sides of Eq. (2) by $H_{l',\mathbf{k}'}$, where $\mathbf{k}'$ is chosen in a neighborhood of $\mathbf{k}_i$, and integrating over the in-plane spatial coordinates gives

$$\sum_j\ c_j \sum_{\mathbf{k}}\ \tilde{\Gamma}_j(\mathbf{k}-\mathbf{k}_j)\langle H_{l',\mathbf{k}'}|(\lambda_{\mathrm{d}}-\lambda_{l,\mathbf{k}}-\hat{\mathcal{L}}'_H)H_{l,\mathbf{k}}\rangle = 0. \tag{11}$$

Using the orthonormality of the Bloch waves and the normalization of their periodic parts described in Eq. (6),

$$\langle H_{l',\mathbf{k}'}|(\lambda_{\mathrm{d}}-\lambda_{l,\mathbf{k}})H_{l,\mathbf{k}}\rangle = (\lambda_{\mathrm{d}}-\lambda_{l,\mathbf{k}})\frac{1}{L^2}\sum_{i=1}^{N}\ e^{i(\mathbf{k}-\mathbf{k}')\cdot\mathbf{R}_i},$$

$$\int_v d^2r\, h^*_{l',\mathbf{k}'}h_{l,\mathbf{k}}e^{i(\mathbf{k}-\mathbf{k}')\cdot\mathbf{r}} = (\lambda_{\mathrm{d}}-\lambda_{l',\mathbf{k}'})\,\delta_{l',l}\delta_{\mathbf{k}',\mathbf{k}}. \tag{12}$$

Note that a reciprocal lattice vector was not included in $\delta_{\mathbf{k}',\mathbf{k}}$ as both $\mathbf{k}'$ and $\mathbf{k}$ (through the localized nature of the $\tilde{\Gamma}_i$) are assumed to lie within a neighborhood of one of the wave vectors comprising the $\star\mathbf{k}$, which by definition are not linked by a reciprocal lattice vector. Equation (11) then simplifies to

$$c_i(\lambda_{\mathrm{d}}-\lambda_{l,\mathbf{k}'})\tilde{\Gamma}_i(\mathbf{k}'-\mathbf{k}_i) - \sum_j\ c_j \sum_{\mathbf{k}}\ \langle H_{l',\mathbf{k}'}|\hat{\mathcal{L}}'_H H_{l,\mathbf{k}}\rangle \times\tilde{\Gamma}_j(\mathbf{k}-\mathbf{k}_j) = 0. \tag{13}$$

Fourier expanding the defect perturbation in reciprocal space,

$$\Delta\eta(\mathbf{r}) = \sum_{\mathbf{k}''}\ \widetilde{\Delta\eta}_{\mathbf{k}''}e^{i\mathbf{k}''\cdot\mathbf{r}}, \tag{14}$$

we can write for the mode-mixing term $\langle H_{l',\mathbf{k}'}|\hat{\mathcal{L}}'_H H_{l,\mathbf{k}}\rangle$ in Eq. (13):

$$\begin{aligned}
&\langle H_{l',\mathbf{k}'}|\hat{\mathcal{L}}'_H H_{l,\mathbf{k}}\rangle \\
&= -\sum_{\mathbf{k}''}\ \left(\sum_{i=1}^{N}\ e^{i(\mathbf{k}+\mathbf{k}''-\mathbf{k}')\cdot\mathbf{R}_i}\frac{\widetilde{\Delta\eta}_{\mathbf{k}''}}{L^2}\int_v d^2r\ \ e^{i(\mathbf{k}+\mathbf{k}''-\mathbf{k}')\cdot\mathbf{r}}\right. \\
&\quad\left.\times h^*_{l',\mathbf{k}'}[i\mathbf{k}''\cdot(\boldsymbol{\nabla}+i\mathbf{k})+\boldsymbol{\nabla}^2+2i\mathbf{k}\cdot\boldsymbol{\nabla}-|\mathbf{k}|^2]h_{l,\mathbf{k}}\right) \\
&= \sum_{\mathbf{G}}\ \sum_{\mathbf{k}''}\ [\widetilde{\Delta\eta}_{\mathbf{k}''}K_{l',l}(\mathbf{k}',\mathbf{k},\mathbf{G}) \\
&\quad + \widetilde{\Delta\eta}_{\mathbf{k}''}(i\mathbf{k}'')\cdot\mathbf{L}_{l',l}(\mathbf{k}',\mathbf{k},\mathbf{G})]\,\delta_{\mathbf{k}'-\mathbf{k}''+\mathbf{G},\mathbf{k}},
\end{aligned} \tag{15}$$

where the $\mathbf{G}$ are reciprocal lattice vectors, and we have defined scalar and vector coupling matrix elements as

$$\begin{aligned}
&K_{l',l}(\mathbf{k}',\mathbf{k},\mathbf{G}) \\
&= -\frac{1}{v}\int_v d^2r e^{i\mathbf{G}\cdot\mathbf{r}}h^*_{l',\mathbf{k}'}(\boldsymbol{\nabla}^2+2i\mathbf{k}\cdot\boldsymbol{\nabla}-|\mathbf{k}|^2)h_{l,\mathbf{k}} \\
&\equiv -\langle h_{l',\mathbf{k}'}|e^{i\mathbf{G}\cdot\mathbf{r}}(\boldsymbol{\nabla}^2+2i\mathbf{k}\cdot\boldsymbol{\nabla}-|\mathbf{k}|^2)|h_{l,\mathbf{k}}\rangle_v
\end{aligned} \tag{16}$$

and

$$\begin{aligned}
\mathbf{L}_{l',l}(\mathbf{k}',\mathbf{k},\mathbf{G}) &= -\frac{1}{v}\int_v d^2r e^{i\mathbf{G}\cdot\mathbf{r}}h^*_{l',\mathbf{k}'}(\boldsymbol{\nabla}+i\mathbf{k})h_{l,\mathbf{k}} \\
&\equiv -\langle h_{l',\mathbf{k}'}|e^{i\mathbf{G}\cdot\mathbf{r}}(\boldsymbol{\nabla}+i\mathbf{k})|h_{l,\mathbf{k}}\rangle_v .
\end{aligned} \tag{17}$$

Substituting Eq. (15) into Eq. (13), keeping only terms that mix states within the lth band, results in the following Fourier space representation of the magnetic field master equation:

$$c_i(\lambda_d-\lambda_{l,\mathbf{k}'})\tilde{\Gamma}_i(\mathbf{k}'-\mathbf{k}_i)$$
$$-\sum_{\mathbf{G}}\sum_j c_j\sum_{\mathbf{k}''}\{[\widetilde{\Delta\eta}_{\mathbf{k}''}K_{l,l}(\mathbf{k}',\mathbf{k}'-\mathbf{k}''+\mathbf{G},\mathbf{G})$$
$$+\widetilde{\Delta\eta}_{\mathbf{k}''}(i\mathbf{k}'')\cdot\mathbf{L}_{l,l}(\mathbf{k}',\mathbf{k}'-\mathbf{k}''+\mathbf{G},\mathbf{G})]$$
$$\times\tilde{\Gamma}_j[(\mathbf{k}'-\mathbf{k}''+\mathbf{G})-\mathbf{k}_j]\}=0. \quad (18)$$

For defect perturbations which are localized in **k**-space as well as in real space, all things being equal the strongest mixing terms will be those with $\mathbf{k}''$ nearest the origin. As such, a further simplification can be made by including only those reciprocal lattice vectors **G** which minimize the magnitude of $\mathbf{k}''$ in coupling the different neighborhoods of the $\star\mathbf{k}$ (satellite extrema). The local mixing of states within the neighborhood of each $\mathbf{k}_i$ will thus be dominated by the Fourier components of $\widetilde{\Delta\eta}$ about the origin with $\mathbf{G}=0$. Similarly, the mixing between neighborhoods of $\mathbf{k}_i$ and $\mathbf{k}_j$, where $i\neq j$, will be dominated by a single **G** which minimizes the magnitude of the vector $\mathbf{G}-(\mathbf{k}_j-\mathbf{k}_i)$. Writing this reciprocal lattice vector as $\mathbf{G}_{j,i}$ and only including the dominant coupling terms in Eq. (18) collapses the sum over **G**, and yields

$$c_i((\lambda_d-\lambda_{l,\mathbf{k}'})\tilde{\Gamma}_i(\mathbf{k}'-\mathbf{k}_i)-\sum_{\mathbf{k}''}[\widetilde{\Delta\eta}_{\mathbf{k}''}K_{l,l}(\mathbf{k}_i,\mathbf{k}_i,\mathbf{0})$$
$$+\widetilde{\Delta\eta}_{\mathbf{k}''}(i\mathbf{k}'')\cdot\mathbf{L}_{l,l}(\mathbf{k}_i,\mathbf{k}_i,\mathbf{0})]\tilde{\Gamma}_i[(\mathbf{k}'-\mathbf{k}'')-\mathbf{k}_i]$$
$$-\sum_{i\neq j}c_j\sum_{\mathbf{k}''}([\widetilde{\Delta\eta}_{\mathbf{k}''}K_{l,l}(\mathbf{k}_i,\mathbf{k}_j,\mathbf{G}_{j,i})+\widetilde{\Delta\eta}_{\mathbf{k}''}(i\mathbf{k}'')$$
$$\cdot\mathbf{L}_{l,l}(\mathbf{k}_i,\mathbf{k}_j,\mathbf{G}_{j,i})]\tilde{\Gamma}_j\{[\mathbf{k}'-(\mathbf{k}''-\mathbf{G}_{j,i})]-\mathbf{k}_j\})=0, \quad (19)$$

where we have neglected the variation of $K_{l,l}$ and $\mathbf{L}_{l,l}$ within the local neighborhoods of the $\mathbf{k}_i\in\star\mathbf{k}$.

Implicit in the derivation of Eq. (19)is that the $\tilde{\Gamma}_i$ are localized around the $\mathbf{k}_i$ in reciprocal space. In order to make this explicit (which will be necessary when transforming back to real-space coordinates)we expand $\lambda_{l,\mathbf{k}'}$ in the vicinity of each $\mathbf{k}_i$,

$$\lambda_{l,\mathbf{k}'}\approx[\lambda_{l,o}+\lambda'_{l,i}(\Delta\mathbf{k})]+O(\Delta k^3), \quad (20)$$

where $\lambda_{l,o}$ is the top (bottom) of the band edge, $\Delta\mathbf{k}=\mathbf{k}'-\mathbf{k}_i$, and $\lambda'_{l,i}$ only contains terms up to second order in elements of $\Delta\mathbf{k}$.[25] In the case of those $\mathbf{k}_i$ located at an extrema of a given (nondegenerate) band the resulting dispersion relation may be written in the form, $\lambda'_{l,i}(\Delta\mathbf{k})=\Delta\mathbf{k}\cdot\mathbf{M}^{-1}_{l,*}\cdot\Delta\mathbf{k}$, where the matrix $\mathbf{M}_{l,*}$ is an effective mass tensor defined by the curvature of the band. Substituting Eq. (20) into Eq. (19) gives

$$c_i\Big((\Delta\lambda_d-\lambda'_{l,i}(\Delta\mathbf{k}))\tilde{\Gamma}_i(\Delta\mathbf{k})-\sum_{\mathbf{k}''}[\widetilde{\Delta\eta}_{\mathbf{k}''}K_{l,l}(\mathbf{k}_i,\mathbf{k}_i,\mathbf{0})$$
$$+\widetilde{\Delta\eta}_{\mathbf{k}''}(i\mathbf{k}'')\cdot\mathbf{L}_{l,l}(\mathbf{k}_i,\mathbf{k}_i,\mathbf{0})]\tilde{\Gamma}_i(\Delta\mathbf{k}-\mathbf{k}'')\Big)$$
$$-\sum_{i\neq j}c_j\sum_{\mathbf{k}''}([\widetilde{\Delta\eta}_{\mathbf{k}''}K_{l,l}(\mathbf{k}_i,\mathbf{k}_j,\mathbf{G}_{j,i})+\widetilde{\Delta\eta}_{\mathbf{k}''}(i\mathbf{k}'')$$
$$\cdot\mathbf{L}_{l,l}(\mathbf{k}_i,\mathbf{k}_j,\mathbf{G}_{j,i})]\tilde{\Gamma}_j[(\Delta\mathbf{k}+\mathbf{G}_{j,i}-\Delta\mathbf{k}_{j,i})-\mathbf{k}'']=0, \quad (21)$$

where $\Delta\lambda_d=\lambda_d-\lambda_{l,o}$ is the eigenvalue referenced to the top (bottom) of the band edge, and $\Delta\mathbf{k}_{j,i}\equiv\mathbf{k}_j-\mathbf{k}_i$.

Equation (21) is the Fourier space representation of an approximate master equation for the localized magnetic field envelope functions of defect states. Transforming back to real space results in a set of coupled Wannier-like equations,

$$c_i\{[\Delta\lambda_d-\lambda'_{l,i}(\hbar^{-1}\hat{\mathbf{p}})]-\Delta\eta'_{i,i}(\mathbf{r})\}\Gamma_i(\mathbf{r})$$
$$-\sum_{i\neq j}c_j(e^{-i(\mathbf{G}_{j,i}-\Delta\mathbf{k}_{j,i})\cdot\mathbf{r}}\Delta\eta'_{j,i}(\mathbf{r}))\Gamma_j(\mathbf{r})=0, \quad (22)$$

$$\Delta\eta'_{j,i}(\mathbf{r})=\Delta\eta(\mathbf{r})K_{l,l}[(\mathbf{k}_i,\mathbf{k}_j,\mathbf{G}_{j,i})$$
$$+\nabla(\Delta\eta(\mathbf{r}))]\cdot\mathbf{L}_{l,l}(\mathbf{k}_i,\mathbf{k}_j,\mathbf{G}_{j,i}), \quad (23)$$

where $\hat{\mathbf{p}}=-i\hbar\nabla$ as in quantum mechanics, and $\Delta\eta'_{j,i}(\mathbf{r})$ is an effective perturbation potential (valid for TE-like modes; see the Appendix for the TM case).

Assuming that the amplitude of the relatively large Fourier components of $\Delta\eta(\mathbf{r})$ associated with mixing of states between neighborhoods of *different* satellite points of the $\star\mathbf{k}$ are much smaller than the amplitude of the small Fourier components which mix states within a given neighborhood of a point of the $\star\mathbf{k}$, we can treat the *inter*-$\mathbf{k}_i$ mixing as a perturbation to the envelope functions formed from the local **k**-space mixing.[30] This allows us to write an independent Wannier-like equation for each of the $\Gamma_i(\mathbf{r})$ envelope functions,

$$\{[\Delta\lambda_d-\lambda'_{l,i}(\hbar^{-1}\hat{\mathbf{p}})]-\Delta\eta'_{i,i}(\mathbf{r})\}\Gamma_i(\mathbf{r})=0. \quad (24)$$

Of most importance for the types of resonant cavities studied here are the ground-state solutions to Eq. (24). This is due to the relatively localized nature of the defect regions. For de-localized defect regions extending over many lattice periods a more extensive set of envelope functions, including higher order functions with added nodes and antinodes must be included. Choice of such a set of envelope functions will depend on the geometry of the boundary of the defect.[32] For the present work then, we take $\Gamma_i(\mathbf{r})$ equal to the ground-state envelope, $\Gamma_{i,o}(\mathbf{r})$.

As the ground state of a system is in general invariant under the symmetries of the Hamiltonian of that system,[30,33] the ground-state envelope function should transform as the identity of the point symmetry group of the Wannier-like

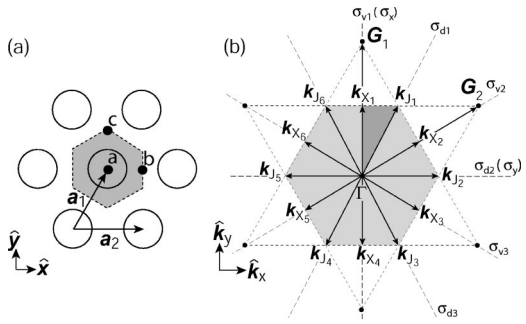

FIG. 2. Illustration of the (a) real and (b) reciprocal spaces of the two-dimensional hexagonal PC ($|\mathbf{a}_1|=|\mathbf{a}_2|=a$, $|\mathbf{G}_1|=|\mathbf{G}_2|=4\pi/\sqrt{3}a$, $|\mathbf{k}_X|=2\pi/\sqrt{3}a$, $|\mathbf{k}_J|=4\pi/3a$). The high-symmetry points of the hexagonal lattice, referenced to the center of an air hole, are $\mathbf{a}=(0,0)$, $\mathbf{b}=(a/2,0)$, and $\mathbf{c}=(0,a/\sqrt{3})$.

equation given in Eq. (24). The spatial symmetries of Eq. (24) are those of $\lambda'_{l,i}(\hbar^{-1}\hat{\mathbf{p}})$ and $\Delta\eta'_{i,i}(\mathbf{r})$. As discussed in Ref. 34, it then follows that the point symmetries of the Wannier-like equation for the ground-state envelope functions are given by $\mathcal{G}'\cap\mathcal{G}'_{\mathbf{k}_i}$, where $\mathcal{G}'$ is the point group of the defect perturbation (independent of the crystal lattice) and $\mathcal{G}'_{\mathbf{k}_i}$ is the point group isomorphic to the group of the wave vector (of the underlying Bravais lattice, not the crystal) at the point $\mathbf{k}_i$ in the first Brillouin zone (IBZ). With this knowledge the coefficients c_i of the defect state in Eq. (10) can then be determined using symmetry arguments.

III. ENVELOPE FUNCTION CALCULATION

Here we will consider two examples of how the Wannier-like equation of the previous section can be used to calculate an approximate envelope function for localized photon state in a hexagonal lattice photonic crystal. The first example consists of a localized donor-type mode formed at the band edge occurring at the X point of the reciprocal lattice where the band structure has a local minimum and is given by a simple paraboloid in a neighborhood of the X point. The second example is that of a localized acceptor-type mode formed from the J-point where the band structure has a local maximum.

For the hexagonal lattice, the high symmetry points within and on the boundary of the IBZ are the six X points ($\{\pm(0,1)k_X,\ \pm(\sqrt{3}/2,1/2)k_X,\ \pm(\sqrt{3}/2,-1/2)k_X\}$), the six J points ($\{\pm(1/2,\sqrt{3}/2)k_J,\ \pm(1/2,-\sqrt{3}/2)k_J,\ \pm(1,0)k_J\}$), and the Γ point$=(0,0)$. The first-order band gap of the hexagonal lattice [see Fig. 1(b)] is defined from above by the X point and below by the J point. In analogy to the electronic bands in semiconductor crystals we term the high frequency band defining the first-order band gap the ''conduction'' band, and the low frequency band the ''valence'' band. In the approximate analysis of the defect states to follow we will need to include all the degenerate satellite peaks (valence band) and valleys (conduction band). For the hexagonal lattice the different degenerate X and degenerate J points on IBZ boundary are labeled as in Fig. 2(b). The group of the wave vector, which defines the point group symmetry of a plane wave modulo $\mathbf{G}$ within the dielectric lattice, is for the X, J, and Γ points of the hexagonal lattice C_{2v}, C_{3v}, and C_{6v}, respectively.[35]

A. Donor modes at the X point

For the frequency bands defining the first-order band-gap, the unpatterned waveguide modes which are most strongly coupled together to form the Bloch modes at the X point are in our quasi-2D picture given by $\mathbf{B}=\hat{z}e^{i\mathbf{k}_{X_i}\cdot\mathbf{r}_\perp}$, with $\mathbf{r}_\perp$ corresponding to coordinates within the symmetry plane of the dielectric slab (for what follows we drop the $\perp$ in labeling the symmetry plane coordinates). The unperturbed frequencies of these modes are degenerate and can be written as $\omega_o^X\approx c|\mathbf{k}_X|/n_{\text{eff}}$, where n_{eff} is an effective index taking into account the vertical waveguiding perpendicular to the slab.

The $\star\mathbf{k}$ at the X point, which is formed from the independent satellite X points within the IBZ, consists (not uniquely) of wave vectors $\{\mathbf{k}_{X_1},\mathbf{k}_{X_2},\mathbf{k}_{X_3}\}$, all other X points being equivalent modulo a reciprocal lattice vector. A symmetry basis for the modes of the patterned slab waveguide at the X_1-satellite point, the irreducible representations (IRREPs) of the little group at the X point, can be found by applying the symmetry operations of the group of the wave vector ($\mathcal{G}_{o\mathbf{k}_X}=C_{2v}$) to the seed vector $\mathbf{B}_{\mathbf{k}_{X_1}}$. In this case, the basis is simply $(\mathbf{B}_{\mathbf{k}_{X_1}},\mathbf{B}_{-\mathbf{k}_{X_1}})$. Projecting this symmetry basis onto the IRREP spaces of C_{2v} yields

$$\mathbf{B}^{X_1}_{A_2}=\hat{z}\cos(\mathbf{k}_{X_1}\cdot\mathbf{r}^a),$$

$$\mathbf{B}^{X_1}_{B_1}=\hat{z}\sin(\mathbf{k}_{X_1}\cdot\mathbf{r}^a), \tag{25}$$

where A_2 and B_1 label the IRREP spaces of C_{2v} (see Ref. 34), and the index a is used to denote the location of the origin within the hexagonal lattice [marked in Fig. 2(a)]. As the magnetic field of $\mathbf{B}^{X_1}_{A_2}$ overlaps strongly with the air holes of the PC (its the electric field lying largely in the dielectric) it describes the lower frequency ''valence'' band mode, while $\mathbf{B}^{X_1}_{B_1}$ describes the ''conduction'' band mode. This is a result of the tendency for modes with the electric field concentrated within regions of high dielectric constant to be lower frequency than those with the electric field concentrated in low dielectric regions.[36]

In order to fully define the modes at the X point all modes of the $\star\mathbf{k}$ must be included. The point symmetry operations of the full point group of the hexagonal lattice not included in the group of the wave vector, the coset generators, may be used to generate the modes of all the degenerate satellite points within the $\star\mathbf{k}$. In the case of the X point this corresponds to successive rotations by $\pi/6$ (C_6 rotation). The result is the following set of three degenerate X-point valence band modes:

$$VB^a_X=\begin{pmatrix} v_{X_1}\\ v_{X_2}\\ v_{X_3}\end{pmatrix}=\hat{z}\begin{pmatrix}\cos(\mathbf{k}_{X_1}\cdot\mathbf{r}^a)\\ \cos(\mathbf{k}_{X_2}\cdot\mathbf{r}^a)\\ \cos(\mathbf{k}_{X_3}\cdot\mathbf{r}^a)\end{pmatrix}, \tag{26}$$

and *X*-point conduction band modes,

$$CB_X^a = \begin{pmatrix} c_{X_1} \\ c_{X_2} \\ c_{X_3} \end{pmatrix} = \hat{z} \begin{pmatrix} \sin(\mathbf{k}_{X_1}\cdot\mathbf{r}^a) \\ \sin(\mathbf{k}_{X_2}\cdot\mathbf{r}^a) \\ \sin(\mathbf{k}_{X_3}\cdot\mathbf{r}^a) \end{pmatrix}. \tag{27}$$

Separating the plane wave and periodic parts of the above Bloch modes allows us to write

$$v_{X_i} = \frac{\hat{z}}{2}(1+e^{-i2\mathbf{k}_{X_i}\cdot\mathbf{r}^a})e^{i\mathbf{k}_{X_i}\cdot\mathbf{r}^a},$$

$$c_{X_i} = \frac{\hat{z}}{i2}(1-e^{-i2\mathbf{k}_{X_i}\cdot\mathbf{r}^a})e^{i\mathbf{k}_{X_i}\cdot\mathbf{r}^a}, \tag{28}$$

with normalized periodic functions given by

$$h_{v,\mathbf{k}_{X_i}} = (1/\sqrt{2})(1+e^{-i2\mathbf{k}_{X_i}\cdot\mathbf{r}^a}),$$

$$h_{c,\mathbf{k}_{X_i}} = (1/i\sqrt{2})(1-e^{-i2\mathbf{k}_{X_i}\cdot\mathbf{r}^a}). \tag{29}$$

We now use the above set of modes to calculate the local dispersion of the conduction band at the *X* point. The Hermitian operator acting on the space of periodic functions at point $\mathbf{k}$ in the reciprocal lattice, for the quasi-2D case studied here, is

$$\hat{\mathcal{L}}_{H,\mathbf{k}} = -\boldsymbol{\nabla}(\eta_o)\cdot(i\mathbf{k}+\boldsymbol{\nabla}) + \eta_o(|\mathbf{k}|^2 - 2i\mathbf{k}\cdot\boldsymbol{\nabla} - \boldsymbol{\nabla}^2), \tag{30}$$

with an associated eigenvalue equation given by

$$\hat{\mathcal{L}}_{H,\mathbf{k}} h_{l,\mathbf{k}} = \lambda_{l,\mathbf{k}} h_{l,\mathbf{k}}. \tag{31}$$

As in "$\mathbf{k}\cdot\hat{\mathbf{p}}$" theory for Bloch electrons in crystalline materials, we expand $\hat{\mathcal{L}}_{H,\mathbf{k}}$ about point $\mathbf{k}_o$,

$$\hat{\mathcal{L}}_{H,\mathbf{k}} = \hat{\mathcal{L}}_{H,\mathbf{k}_o} + \hat{\mathcal{L}}'_{H,\Delta\mathbf{k}}, \tag{32}$$

with

$$\hat{\mathcal{L}}'_{H,\Delta\mathbf{k}} \equiv \eta_o|\Delta\mathbf{k}|^2 + \Delta\mathbf{k}\cdot[-i\boldsymbol{\nabla}(\eta_o) + 2\eta_o\mathbf{k}_o - 2i\eta_o\boldsymbol{\nabla}]. \tag{33}$$

Treating $\hat{\mathcal{L}}'_{H,\Delta\mathbf{k}}$ as a perturbation to $\hat{\mathcal{L}}_{H,\mathbf{k}_o}$, and expanding $h_{l,\mathbf{k}}$ in terms of the $h_{l,\mathbf{k}_o}$,[40] gives, to second order in elements of $\Delta\mathbf{k}$,

$$\lambda_{l,\mathbf{k}\sim\mathbf{k}_o} = \lambda_{l,\mathbf{k}_o} + \Delta\mathbf{k}\cdot\langle h_{l,\mathbf{k}_o}|[-i\boldsymbol{\nabla}(\eta_o) + 2\eta_o\mathbf{k}_o - 2i\eta_o\boldsymbol{\nabla}]|h_{l,\mathbf{k}_o}\rangle_v + |\Delta\mathbf{k}|^2\langle h_{l,\mathbf{k}_o}|\eta_o|h_{l,\mathbf{k}_o}\rangle_v + \sum_{l'\neq l}\frac{|\Delta\mathbf{k}\cdot\langle h_{l',\mathbf{k}_o}|[-i\boldsymbol{\nabla}(\eta_o) + 2\eta_o\mathbf{k}_o - 2i\eta_o\boldsymbol{\nabla}]|h_{l,\mathbf{k}_o}\rangle_v|^2}{(\lambda_{l,\mathbf{k}_o} - \lambda_{l',\mathbf{k}_o})}. \tag{34}$$

If $\mathbf{k}_o$ corresponds to an extremal point within the band structure, then the linear $\Delta\mathbf{k}$ terms in the Eq. (34) are identically zero. One can check that for the *X*-point conduction and valence band modes of Eq. (28) that this is indeed the case. Substituting the periodic functions of the conduction and valence band modes of Eq. (29) into Eq. (34) gives, for the local *X*-point band structure of the conduction band,

$$\lambda_{c,\mathbf{k}\sim\mathbf{k}_{X_i}} = \lambda_{c,\mathbf{k}_{X_i}} + |\Delta\mathbf{k}|^2\langle h_{c,\mathbf{k}_{X_i}}|\eta_o|h_{c,\mathbf{k}_{X_i}}\rangle_v + \frac{|\Delta\mathbf{k}\cdot\langle h_{v,\mathbf{k}_{X_i}}|[-i\boldsymbol{\nabla}(\eta_o) + 2\eta_o\mathbf{k}_{X_i} - 2i\eta_o\boldsymbol{\nabla}]|h_{c,\mathbf{k}_{X_i}}\rangle_v|^2}{\Delta\lambda_X}, \tag{35}$$

where $\Delta\lambda_X \equiv (\lambda_{c,\mathbf{k}_X} - \lambda_{v,\mathbf{k}_X})$.

Fourier expanding η_o,

$$\eta_o = \sum_{\mathbf{G}} \tilde{\eta}_{o,\mathbf{G}} e^{i\mathbf{G}\cdot\mathbf{r}^a}, \tag{36}$$

allows the band structure to be evaluated in terms of the Fourier coefficients of the dielectric PC. Since η_o is a lattice periodic *real* function, $\mathbf{G}$ are reciprocal lattice vectors and $\tilde{\eta}_{o,\mathbf{G}} = (\tilde{\eta}_{o,-\mathbf{G}})^*$. With the origin located at point *a* of the lattice [see Fig. 2(a)], the hexagonal PC has a C_{6v} symmetry. As a result the Fourier coefficients of the hexagonal lattice are all real (inversion symmetry of the lattice), and $\tilde{\eta}_{o,2\mathbf{k}_{X_i}} = \tilde{\eta}_{o,2\mathbf{k}_{X_j}}$, for all $\mathbf{k}_{X_i},\mathbf{k}_{X_j} \in \star\mathbf{k}$. Also, as point *a* lies within the center of an air hole, the fundamental Fourier coefficients of the lattice, $\tilde{\eta}_{o,2\mathbf{k}_{X_i}}$, must be positive. Substituting Eq. (36) into Eq. (35) gives

$$\lambda_{c,\mathbf{k}\sim\mathbf{k}_{X_i}} = \lambda_{c,\mathbf{k}_X} + |\Delta\mathbf{k}|^2(\tilde{\eta}_{o,\mathbf{0}} - \tilde{\eta}_{o,2\mathbf{k}_X}) + \frac{4|(\Delta\mathbf{k}\cdot\mathbf{k}_{X_i})|^2(\tilde{\eta}_{o,\mathbf{0}})^2}{\Delta\lambda_X}, \tag{37}$$

where the index *i* has been dropped from $\mathbf{k}_{X_i}$ in those quantities that have the same value for each element of the $\star\mathbf{k}$.

The band gap at the X point, $\Delta\lambda_X$, may also be approximately determined in terms of the Fourier coefficients $\tilde{\eta}_{o,\mathbf{G}}$. The magnetic field eigenoperator $\hat{\mathcal{L}}_H$ can be written as

$$\hat{\mathcal{L}}_H = -\tilde{\eta}_{o,\mathbf{0}}\nabla^2 - \sum_{\mathbf{G}\neq 0} \tilde{\eta}_{o,\mathbf{G}} e^{i\mathbf{G}\cdot\mathbf{r}}[\nabla^2 + i\tilde{\eta}_{o,\mathbf{G}}\mathbf{G}\cdot\nabla]. \tag{38}$$

Treating $\Delta\eta_o = \Sigma_{\mathbf{G}\neq 0}\tilde{\eta}_{o,\mathbf{G}}e^{i\mathbf{G}\cdot\mathbf{r}}$ as a perturbation to the average dielectric $\tilde{\eta}_{o,\mathbf{0}}$, and considering only the coupling between the forward and backward normalized plane wave states at the X point, $(|\mathbf{k}_{X_i}\rangle, |-\mathbf{k}_{X_i}\rangle)$, results in the following two band magnetic field eigenoperator:

$$\hat{\mathcal{L}}_H^{X_i} = \begin{pmatrix} \tilde{\eta}_{o,\mathbf{0}}|\mathbf{k}_X|^2 & -\tilde{\eta}_{o,2\mathbf{k}_X}|\mathbf{k}_X|^2 \\ -\tilde{\eta}_{o,2\mathbf{k}_X}|\mathbf{k}_X|^2 & \tilde{\eta}_{o,\mathbf{0}}|\mathbf{k}_X|^2 \end{pmatrix}. \tag{39}$$

The eigenvalues of $\hat{\mathcal{L}}_H^{X_i}$ are $\tilde{\eta}_{o,\mathbf{0}}|\mathbf{k}_X|^2 \pm (\tilde{\eta}_{o,2\mathbf{k}_X})|\mathbf{k}_X|^2$, which gives for the band gap, $\Delta\lambda_X = 2(\tilde{\eta}_{o,2\mathbf{k}_X})|\mathbf{k}_X|^2$.

Choosing a coordinate basis $\hat{\mathbf{x}}_i$ with $\hat{x}_i$ orthogonal to $\mathbf{k}_{X_i}$ and $\hat{y}_i$ parallel to $\mathbf{k}_{X_i}$, allows us to write for the local band structure of the conduction band in the vicinity of the X_i point,

$$\lambda_{c,\mathbf{k}\sim\mathbf{k}_{X_i}} = \lambda_{c,\mathbf{k}_X} + \frac{\Delta\mathbf{k}_{x_i}^2}{m^*_{c,X,x_i}} + \frac{\Delta\mathbf{k}_{y_i}^2}{m^*_{c,X,y_i}}, \tag{40}$$

with effective "masses"[41] defined as

$$\frac{1}{m^*_{c,X,x_i}} = \tilde{\eta}_{o,\mathbf{0}}\left(1 - \frac{\tilde{\eta}_{o,2\mathbf{k}_X}}{\tilde{\eta}_{o,\mathbf{0}}}\right),$$

$$\frac{1}{m^*_{c,X,y_i}} = \tilde{\eta}_{o,\mathbf{0}}\left(1 - \frac{\tilde{\eta}_{o,2\mathbf{k}_X}}{\tilde{\eta}_{o,\mathbf{0}}} + \frac{2\tilde{\eta}_{o,\mathbf{0}}}{\tilde{\eta}_{o,2\mathbf{k}_X}}\right). \tag{41}$$

For a PC formed from dielectric materials with real refractive indices greater than that of vacuum, $0 \leqslant \eta_o(\mathbf{r}) \leqslant 1$. Consequently, $\tilde{\eta}_{o,\mathbf{0}} \geqslant 0$ and $\tilde{\eta}_{o,\mathbf{0}} \geqslant 2\tilde{\eta}_{o,\mathbf{G}}$ for all $\mathbf{G}$. The effective masses for the conduction band at the X-point are thus both positive.

Evaluating the scalar and vector coupling matrix elements using the X_i-point conduction band modes of Eq. (29) gives $K_{l,l}(\mathbf{k}_{X_i},\mathbf{k}_{X_i},\mathbf{0}) = |\mathbf{k}_X|^2$ and $\mathbf{L}_{l,l}(\mathbf{k}_{X_i},\mathbf{k}_{X_i},\mathbf{0}) = \mathbf{0}$. Substituting these coupling matrix elements into Eq. (23), the effective Wannier potential is

$$\Delta\eta'_{i,i}(\mathbf{r}) = |\mathbf{k}_X|^2 \Delta\eta(\mathbf{r}). \tag{42}$$

Lastly, upon substituting the local band structure of Eq. (40) and the effective Wannier potential of Eq. (42) into Eq. (24), for the Wannier equation of the conduction band envelope at the ith X point we have

$$\left[(\lambda_d - \lambda_{c,\mathbf{k}_X}) - \left(\frac{-\nabla_{x_i}^2}{m^*_{c,X,x_i}} + \frac{-\nabla_{y_i}^2}{m^*_{c,X,y_i}} + |\mathbf{k}_X|^2\Delta\eta(\mathbf{r})\right)\right]\Gamma_{c,\mathbf{k}_{X_i}}(\mathbf{r}) = 0. \tag{43}$$

We now see from the Wannier-like equation for the conduction band edge at the X point that as a result of the positive effective mass coefficients, localized resonant modes will form for perturbations to the hexagonal lattice in which $\Delta\eta(\mathbf{r})$ is locally reduced, that is for which the refractive index is locally *increased*.

Here we consider a defect which results in an approximate harmonic perturbation potential. By appropriately varying the hole radii of a photonic crystal consisting of a hexagonal array of air holes in a host dielectric material, the inverse of the filling fraction of the hexagonal crystal can be graded in a roughly parabolic fashion. The filling fraction of the lattice, f, as a function of air hole radius is

$$f = 1 - \frac{2\pi}{\sqrt{3}}\left(\frac{r}{a}\right)^2, \tag{44}$$

where r is the hole radius and a is the nearest neighbor distance between holes of the hexagonal lattice. For a host dielectric material of refractive index n_o, the average dielectric constant of the patterned crystal is $\overline{\epsilon} = f(n_o)^2$. The slowly varying envelope of η_o ($\overline{\eta_o}$), neglecting rapid variations on the scale of the lattice spacing, is proportional to $1/f$, $\overline{\eta_o} = (n_o)^{-2}/f$. For an approximate harmonic potential then, the filling fraction of the lattice should vary as

$$\frac{1}{f(\rho)} = \frac{1}{f_o} + k\left(\frac{\rho}{a}\right)^2, \tag{45}$$

with ρ representing the radial distance from the center of the defect, f_o the filling fraction given by the air hole radius at the center of the defect, and k the lattice grading coefficient. The filling fraction as used here is a local approximation, based upon the local hole radius, to the true filling fraction of a crystal lattice. The resulting slowly varying envelope of the effective Wannier potential is

$$\overline{\Delta\eta'}_{i,i}(\rho) = k\left(\frac{\rho}{a}\right)^2\left(\frac{|\mathbf{k}_X|}{n_o}\right)^2. \tag{46}$$

The ground-state solution to Eq. (43) with the harmonic effective potential of Eq. (46) is the 2D Gaussian,

$$\Gamma_{c,\mathbf{k}_{X_i}}(\mathbf{r}) = \exp[-(x_i^2/\kappa^2 + y_i^2/\gamma^2)], \tag{47}$$

with decay constants

$$\frac{1}{\kappa^2} = \frac{1}{2}(\overline{k}\ m^*_{c,X,x_i})^{1/2},$$

$$\frac{1}{\gamma^2} = \frac{1}{2}(\overline{k}\ m^*_{c,X,y_i})^{1/2}, \tag{48}$$

TABLE I. Hexagonal PC parameters for the donor- and acceptor-type defect cavities.

cavity	n_o	$\left(\frac{r}{a}\right)_o$	f_o	k	$\overline{k}/a^2$	$\left(\frac{r}{a}\right)_e$	$\frac{\tilde{\eta}_{o,2\mathbf{k}_X}}{\tilde{\eta}_{o,\mathbf{0}}}$
donor	2.65	0.25	0.77	0.01	0.019	0.4	0.294
acc.	2.65	0.35	0.56	−0.006	0.015	0.20	0.23

where $\overline{k}=k(|\mathbf{k}_X|/an_o)^2$.

From Eq. (44), in order to obtain the parabolic grade in filling fraction the normalized hole radius of the defect cavity must vary with ρ as

$$\left(\frac{r}{a}\right)^2=\frac{\sqrt{3}}{2\pi}\left(1-f_o\frac{1}{1+f_ok(\rho/a)^2}\right). \tag{49}$$

With grading parameters given in Table I, the donor-type defect cavity we consider here is plotted in Fig. 3(a). The calculated parameters of the approximate envelope function for the donor modes of this defect cavity are given in Table II.

The point group symmetry of the donor-type defect cavity of Fig. 3(a) centered about point *a* of the hexagonal lattice is that of the underlying hexagonal lattice, C_{6v}. From the character values of the representation of the CB_X^a basis under the C_{6v} point group,[34] we find that this representation decomposes as $E_1\oplus B_1''$. Projecting the CB_X^a basis onto its IRREPs,[35] a set of basis functions for the localized conduction band donor modes is found:

$$\mathbf{B}_{B_1''}^{a,d1}=|c_{X_1}\rangle\Gamma_{c,\mathbf{k}_{X_1}}-|c_{X_2}\rangle\Gamma_{c,\mathbf{k}_{X_2}}+|c_{X_3}\rangle\Gamma_{c,\mathbf{k}_{X_3}},$$

$$\mathbf{B}_{E_1,1}^{a,d1}=2|c_{X_1}\rangle\Gamma_{c,\mathbf{k}_{X_1}}+|c_{X_2}\rangle\Gamma_{c,\mathbf{k}_{X_2}}-|c_{X_3}\rangle\Gamma_{c,\mathbf{k}_{X_3}}, \tag{50}$$

$$\mathbf{B}_{E_1,2}^{a,d1}=|c_{X_2}\rangle\Gamma_{c,\mathbf{k}_{X_2}}+|c_{X_3}\rangle\Gamma_{c,\mathbf{k}_{X_3}}.$$

In Figs. 4(a) and 4(b) the magnetic field intensity is plotted for the dipolelike modes of the E_1 IRREP with envelope functions given by the $\Gamma_{c,\mathbf{k}_{X_i}}$ of Eq. (47). The calculated decay parameters for the Gaussian $\Gamma_{c,\mathbf{k}_{X_i}}$ are tabulated in

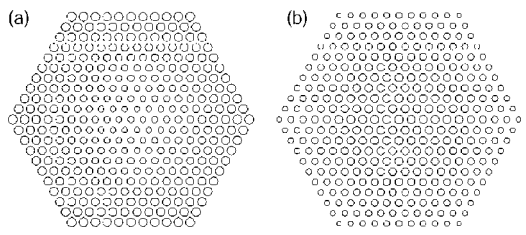

FIG. 3. (a) Graded hexagonal lattice donor-type cavity, (b) graded hexagonal lattice acceptor-type cavity (parameters are given in Table I).

TABLE II. Donor mode (X point) ground-state Wannier envelope parameters.

m_{c,X,x_i}^*	m_{c,X,y_i}^*	$\frac{\kappa}{a}$	$\frac{\gamma}{a}$
7.7	0.72	2.3	4.1

Table II. Note that the coefficients of the expansion for each donor mode (c_i) are determined solely by the transformation properties of the basis CB_X^a; the envelope functions transform effectively as the identity and do not modify the expansion coefficients. This holds in general for envelope functions given by the ground-state solution of the Wannier-like equation.[34]

For comparison, 2D FDTD simulations were performed on the donor-type cavity of Fig. 3(a). Details of the FDTD calculation can be found in other work.[37] Plots of the FDTD calculated magnetic field patterns of the two modes most deep within the first order band gap are given in Figs. 4(c) and 4(d). The modes transform as the B_1'' and B_2'' IRREPs of the C_{2v} point group (the FDTD simulation was performed with mirror plane symmetries to reduce the size of the computation, thus projecting the modes onto the C_{2v} IRREPs), equivalent to the $\hat{x}$ and $\hat{y}$ basis of the C_{6v} IRREP E_1 (the basis chosen for modes $\mathbf{B}_{E_1,1}^{a,d1}$ and $\mathbf{B}_{E_1,2}^{a,d1}$). Along with a match of the symmetry of the modes, the FDTD generated field patterns also show good correspondence to the field patterns of the approximate symmetry analysis [Figs. 4(a)and 4(b)].

A more quantitative estimate of the envelope of the FDTD generated localized modes can be obtained by considering the form of the approximate symmetry analysis modes of Eqs. (50) and (27). Multiplying a donor mode which contains a dominant Fourier component at $\mathbf{k}_{X_i}$ by $\cos(\mathbf{k}_{X_i}\cdot\mathbf{r}^a)$ will produce a term proportional to $\Gamma_{c,\mathbf{k}_{X_i}}$, thus shifting the envelope to the origin in Fourier space. Applying a low-pass spatial filter to the product of the mode and the cosine function will then leave only the envelope corresponding to $\Gamma_{c,\mathbf{k}_{X_i}}$. In Figs. 4(f)–4(h) we plot the result of such a procedure applied to the FDTD calculated $\mathbf{B}_{E_1,1}^{a,d1}$ (x-dipole) mode [Fig. 4(e) shows a plot of the envelope calculated using the Wannier-like equation]. The FDTD generated envelope (corresponding to $\Gamma_{c,\mathbf{k}_{X_1}}$) is oriented parallel to $\mathbf{k}_{X_1}$, and, as can be seen from Figs. 4(g) and 4(h), is Gaussian in nature. The fit decay parameters along $\hat{x}_i$ and $\hat{y}_i$ directions are given in Table III, and although smaller than estimated (Table II), they are in nearly the precise ratio predicted by the Wannier equation.

B. Acceptor modes at the *J* point

As mentioned above, the valence band edge of the fundamental band gap for TE-like modes occurs at the *J* point of the reciprocal lattice for the hexagonal PC. The degenerate

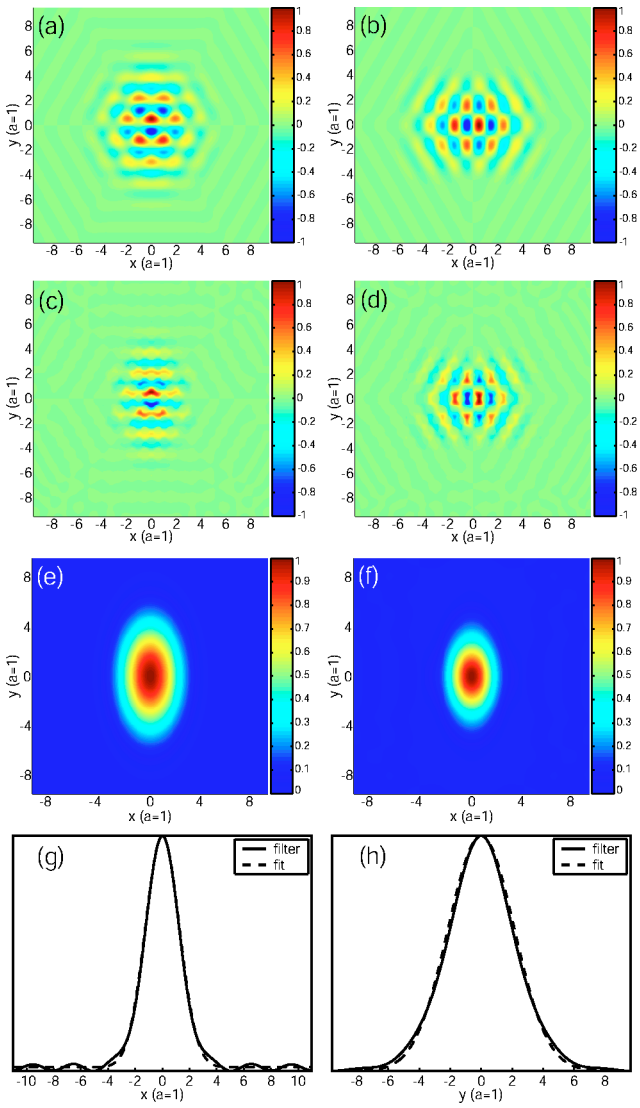

FIG. 4. Magnetic field ($\hat{z}$-component) plot of the donor modes of the graded hexagonal donor-type cavity: (a) the symmetry analysis $B^{a,d1}_{E_1,1}$ (x-dipole) mode, (b) the symmetry analysis $B^{a,d1}_{E_1,2}$ (y-dipole) mode, (c) the FDTD simulated x-dipole mode, and (d) the FDTD simulated y-dipole mode. A comparison of (e) Wannier and (f) FDTD envelope functions for $\mathbf{B}^{d,a1}_{E_1,1}$ (x-dipole) donor mode. (g) and (h) shows line scans of the FDTD filtered envelope (solid line) along the $\hat{x}$ and $\hat{y}$ directions, respectively. The Gaussian fit to the FDTD envelope along these principal directions are also plotted (dashed line)

.

modes of the unpatterned waveguide which most strongly couple together to form the lowest frequency Bloch modes at the J point have magnetic field given approximately by $\mathbf{B}=\hat{z}e^{i\mathbf{k}_{J_i}\cdot\mathbf{r}}$. The $\star\mathbf{k}$ at the J point consists (not uniquely) of $\{\mathbf{k}_{J_1},\mathbf{k}_{J_2}\}$, and the group of the wave vector is $\mathcal{G}_{o\mathbf{k}_J}=C_{3v}$. Using a similar procedure as that described above for the X-point Bloch modes of the fundamental band gap, gives for the approximate TE-like J-point valence band modes (with point a taken as the origin)

TABLE III. FDTD calculated mode envelope parameters.

Mode	$\frac{\kappa}{a}\left(\frac{\kappa_x}{a}\right)$	$\frac{\gamma}{a}\left(\frac{\kappa_y}{a}\right)$
$\mathbf{B}^{a,d1}_{E_1,1}$	1.77	3.02
$\mathbf{B}^{a,a1}_{A_2}$	4.65	4.52
$\mathbf{B}^{a,a1}_{B_2}$	5.29	4.48

$$VB^a_J=\begin{pmatrix} v_{J_1}\\ v_{J_2}\end{pmatrix}=\hat{z}\begin{pmatrix} e^{i\mathbf{k}_{J_1}\cdot\mathbf{r}^a}+e^{i\mathbf{k}_{J_3}\cdot\mathbf{r}^a}+e^{i\mathbf{k}_{J_5}\cdot\mathbf{r}^a}\\ e^{i\mathbf{k}_{J_2}\cdot\mathbf{r}^a}+e^{i\mathbf{k}_{J_4}\cdot\mathbf{r}^a}+e^{i\mathbf{k}_{J_6}\cdot\mathbf{r}^a}\end{pmatrix} \tag{51}$$

and J-point conduction band modes

$$CB^a_J=\begin{pmatrix} c1_{J_1}\\ c2_{J_1}\\ c1_{J_2}\\ c2_{J_2}\end{pmatrix}=\hat{z}\begin{pmatrix} e^{-i\mathbf{k}_{J_1}\cdot\mathbf{r}^a}+e^{-i\mathbf{k}_{J_3}\cdot\mathbf{r}^a}-2e^{-i\mathbf{k}_{J_5}\cdot\mathbf{r}^a}\\ e^{-i\mathbf{k}_{J_1}\cdot\mathbf{r}^a}-e^{-i\mathbf{k}_{J_3}\cdot\mathbf{r}^a}\\ e^{-i\mathbf{k}_{J_2}\cdot\mathbf{r}^a}+e^{-i\mathbf{k}_{J_4}\cdot\mathbf{r}^a}-2e^{-i\mathbf{k}_{J_6}\cdot\mathbf{r}^a}\\ e^{-i\mathbf{k}_{J_2}\cdot\mathbf{r}^a}-e^{-i\mathbf{k}_{J_4}\cdot\mathbf{r}^a}\end{pmatrix}. \tag{52}$$

Note that the conduction band at the J point is doubly degenerate, the bands labeled as $c1$ and $c2$, also a property of the numerically calculated band structure of Fig. 1(b). The normalized periodic functions of the above Bloch modes are

$$h_{v,\mathbf{k}_{J_1}}=\frac{1}{\sqrt{3}}(1+e^{-i2\mathbf{k}_{X_1}\cdot\mathbf{r}^a}+e^{-i2\mathbf{k}_{X_2}\cdot\mathbf{r}^a}),$$

$$h_{v,\mathbf{k}_{J_2}}=\frac{1}{\sqrt{3}}(1+e^{-i2\mathbf{k}_{X_2}\cdot\mathbf{r}^a}+e^{-i2\mathbf{k}_{X_3}\cdot\mathbf{r}^a}), \tag{53}$$

$$h_{c1,\mathbf{k}_{J_1}}=\frac{1}{\sqrt{6}}(1+e^{-i2\mathbf{k}_{X_1}\cdot\mathbf{r}^a}-2e^{-i2\mathbf{k}_{X_2}\cdot\mathbf{r}^a}),$$

$$h_{c1,\mathbf{k}_{J_2}}=\frac{1}{\sqrt{6}}(1+e^{-i2\mathbf{k}_{X_2}\cdot\mathbf{r}^a}-2e^{-i2\mathbf{k}_{X_3}\cdot\mathbf{r}^a}), \tag{54}$$

$$h_{c2,\mathbf{k}_{J_1}}=\frac{1}{\sqrt{2}}(1-e^{-i2\mathbf{k}_{X_1}\cdot\mathbf{r}^a}),$$

$$h_{c2,\mathbf{k}_{J_2}}=\frac{1}{\sqrt{2}}(1-e^{-i2\mathbf{k}_{X_2}\cdot\mathbf{r}^a}). \tag{55}$$

The local band structure for the valence band at the J_1 point, upon evaluating Eq. (34) using the above approximate J_1-point valence and conduction band modes, is

$$\lambda_{v,\mathbf{k}\sim\mathbf{k}_{J_1}}=\lambda_{v,\mathbf{k}_J}+|\Delta\mathbf{k}|^2(\tilde{\eta}_{o,\mathbf{0}}+2\tilde{\eta}_{o,2\mathbf{k}_X})-\left(|\Delta\mathbf{k}\cdot\mathbf{k}_{J_2}|^2\frac{[2(\tilde{\eta}_{o,\mathbf{0}})^2+\frac{1}{2}(\tilde{\eta}_{o,2\mathbf{k}_X})^2+2(\tilde{\eta}_{o,\mathbf{0}})(\tilde{\eta}_{o,2\mathbf{k}_X})]}{\Delta\lambda_J}\right.$$
$$\left.+\frac{4}{3}|\Delta\mathbf{k}\cdot\mathbf{k}_{X_1}|^2\frac{[2(\tilde{\eta}_{o,\mathbf{0}})^2+\frac{1}{2}(\tilde{\eta}_{o,2\mathbf{k}_X})^2+2(\tilde{\eta}_{o,\mathbf{0}})(\tilde{\eta}_{o,2\mathbf{k}_X})]}{\Delta\lambda_J}\right)$$
$$=\lambda_{v,\mathbf{k}_J}+|\Delta\mathbf{k}|^2\left(\tilde{\eta}_{o,\mathbf{0}}+2\tilde{\eta}_{o,2\mathbf{k}_X}-\frac{|\mathbf{k}_J|^2[2(\tilde{\eta}_{o,\mathbf{0}})^2+\frac{1}{2}(\tilde{\eta}_{o,2\mathbf{k}_X})^2+2(\tilde{\eta}_{o,\mathbf{0}})(\tilde{\eta}_{o,2\mathbf{k}_X})]}{\Delta\lambda_J}\right), \tag{56}$$

where $\Delta\mathbf{k}=\mathbf{k}-\mathbf{k}_{J_1}$. To second order in the elements of $\Delta\mathbf{k}$ the local band structure around the J_1 point of the valence band is centrosymmetric. As a result, the local band structure in the neighborhood of each of the J points of the $\star\mathbf{k}$ is also given by Eq. (56). In order to determine the sign of the curvature of the valence band, the band gap at the J point, $\Delta\lambda_J$, is evaluated using a similar procedure as for the band gap at the X point. The three band eigenoperator, in the normalized plane wave basis of $(|\mathbf{k}_{J_1}\rangle,|\mathbf{k}_{J_3}\rangle,|\mathbf{k}_{J_5}\rangle)$, is

$$\hat{\mathcal{L}}_H^{J_1}=|\mathbf{k}_J|^2\begin{pmatrix}\tilde{\eta}_{o,\mathbf{0}} & -\frac{1}{2}\tilde{\eta}_{o,2\mathbf{k}_X} & -\frac{1}{2}\tilde{\eta}_{o,2\mathbf{k}_X}\\ -\frac{1}{2}\tilde{\eta}_{o,2\mathbf{k}_X} & \tilde{\eta}_{o,\mathbf{0}} & -\frac{1}{2}\tilde{\eta}_{o,2\mathbf{k}_X}\\ -\frac{1}{2}\tilde{\eta}_{o,2\mathbf{k}_X} & -\frac{1}{2}\tilde{\eta}_{o,2\mathbf{k}_X} & \tilde{\eta}_{o,\mathbf{0}}\end{pmatrix}. \tag{57}$$

The eigenvalues of $\hat{\mathcal{L}}_H^{J_1}$ consist of the single eigenvalue $\lambda_{v,\mathbf{k}_J}=|\mathbf{k}_J|^2(\tilde{\eta}_{o,\mathbf{0}}-\tilde{\eta}_{o,2\mathbf{k}_X})$, and the double eigenvalue $\lambda_{c,\mathbf{k}_J}=|\mathbf{k}_J|^2(\tilde{\eta}_{o,\mathbf{0}}+\tilde{\eta}_{o,2\mathbf{k}_X}/2)$. The band gap at the J point is then, $\Delta\lambda_J=(3/2)\tilde{\eta}_{o,2\mathbf{k}_X}|\mathbf{k}_J|^2$. Substituting this value of $\Delta\lambda_J$ into Eq. (56) we have, for the local band structure at each of the J points,

$$\lambda_{v,\mathbf{k}\sim\mathbf{k}_J}=\lambda_{v,\mathbf{k}_J}+\frac{|\Delta\mathbf{k}|^2}{m^*_{v,J}}. \tag{58}$$

where the effective mass of the valence band is

$$\frac{1}{m^*_{v,J}}=-\frac{1}{3}\tilde{\eta}_{o,\mathbf{0}}\left(1+3\frac{\tilde{\eta}_{o,2\mathbf{k}_X}}{\tilde{\eta}_{o,\mathbf{0}}}+\frac{4[(\tilde{\eta}_{o,\mathbf{0}})^2-2(\tilde{\eta}_{o,2\mathbf{k}_X})^2]}{(\tilde{\eta}_{o,\mathbf{0}})(\tilde{\eta}_{o,2\mathbf{k}_X})}\right). \tag{59}$$

As expected for the valence band, the effective mass is negative at the J point.

The scalar and vector coupling matrix elements, evaluated using the J_1-point valence band mode of eq. (53), are $K_{v,v}(\mathbf{k}_{J_1},\mathbf{k}_{J_1},\mathbf{0})=|\mathbf{k}_J|^2$ and $\mathbf{L}_{v,v}(\mathbf{k}_{J_1},\mathbf{k}_{J_1},\mathbf{0})=\mathbf{0}$. The resulting effective Wannier potential at the J point is given by

$$\Delta\eta'_{i,i}(\mathbf{r})=|\mathbf{k}_J|^2\Delta\eta(\mathbf{r}). \tag{60}$$

With the local band structure of Eq. (58) and the effective potential of eq. (60), the Wannier equation of the valence band envelope at the J point is

$$\left[(\lambda_d-\lambda_{v,\mathbf{k}_J})-\left(\frac{-\boldsymbol{\nabla}^2}{m^*_{v,J}}+|\mathbf{k}_J|^2\Delta\eta(\mathbf{r})\right)\right]\Gamma_{v,\mathbf{k}_J}(\mathbf{r})=0. \tag{61}$$

Due to the negative effective mass coefficient, localized resonant modes will form for local perturbations to the hexagonal lattice in which the refractive index is locally *decreased*. The acceptor-type defect is taken to consist of a grade in the radius of the air holes of the hexagonal crystal as defined in Eq. (49), with grading coefficient $k=-0.006$. The values of the parameters of the acceptor-type cavity are given in Table I and a plot of the acceptor-type cavity is shown in Fig. 3(b).

As was the case for the donor-type cavity, this grade in the hole radius results in an approximate parabolic potential well. Therefore, we take as our approximate ground-state envelope function the Gaussian

$$\Gamma_{v,\mathbf{k}_J}(\mathbf{r})=\exp[-(\rho/\kappa)^2], \tag{62}$$

with $\rho=|\mathbf{r}_\perp|$ the in-plane radius, and κ a single parameter decay constant given by

$$\frac{1}{\kappa^2}=\frac{1}{2}(\bar{k}\ |m^*_{v,J}|)^{1/2}, \tag{63}$$

where $\bar{k}=|k|(|\mathbf{k}_J|/an_o)^2$. The value of κ/a as calculated for the acceptor-type defect of Figure 3(b) is given in Table IV.

From the character values of the representation of VB_J^a under the C_{6v} point symmetry group, VB_J^a decomposes into irreducible blocks $A_2''\oplus B_2''$. Projecting the basis VB_J^a onto its IRREPS, the localized acceptor modes are

$$\mathbf{B}^{a,a1}_{A_2''}=|v_{J_1}\rangle\Gamma_{v,\mathbf{k}_J}+|v_{J_2}\rangle\Gamma_{v,\mathbf{k}_J}\propto\hat{z}[\cos(\mathbf{k}_{J_1}\cdot\mathbf{r})+\cos(\mathbf{k}_{J_2}\cdot\mathbf{r})$$
$$+\cos(\mathbf{k}_{J_3}\cdot\mathbf{r})]\Gamma_{v,\mathbf{k}_J}, \tag{64}$$

TABLE IV. Acceptor mode (J-point) ground-state Wannier envelope parameters.

$m^*_{v,J}$	$\frac{\kappa}{a}=\frac{\kappa_x}{a}=\frac{\kappa_y}{a}$
-0.68	4.44

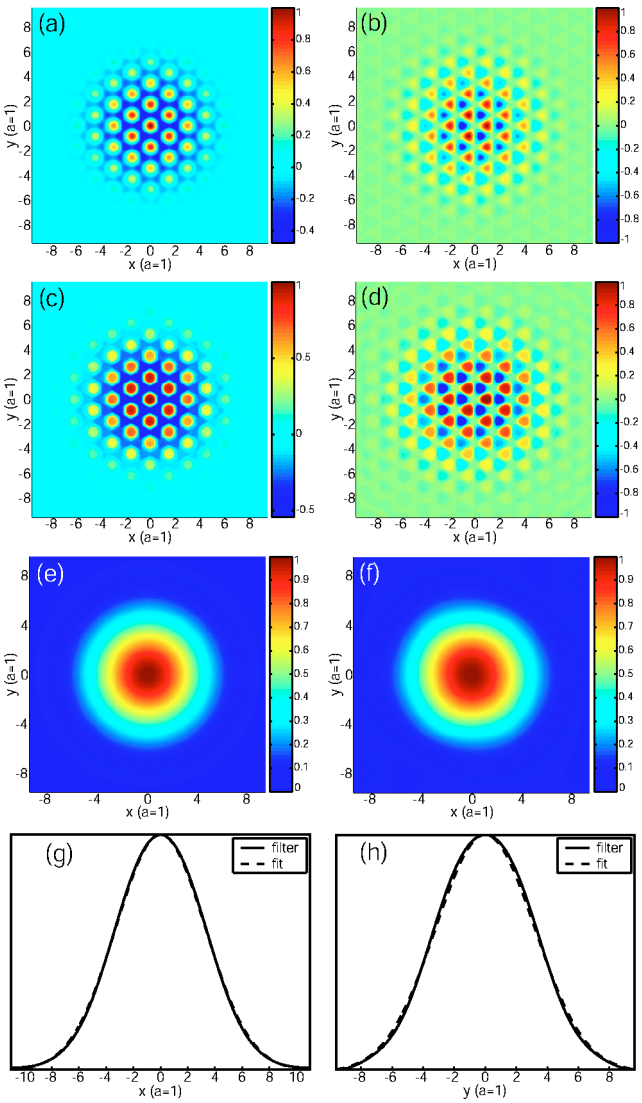

FIG. 5. Magnetic field ($\hat{z}$ component) plots of the acceptor modes of the graded hexagonal lattice acceptor-type cavity: (a) symmetry analysis A_2'' mode, (b) symmetry analysis B_2'' mode, (c) FDTD A_2'' mode, and (d) FFDTD B_2'' mode. Comparison of (e) Wannier (see Table IV) and (f) FDTD envelope functions for the $\mathbf{B}_{A_2}^{a,a1}$ acceptor mode. (g) and (h) show line scans of the FDTD filtered envelope (solid line) along the $\hat{x}$ and $\hat{y}$ directions, respectively. The Gaussian fit to the FDTD envelope along these principal directions are also plotted (dashed line).

$$\mathbf{B}_{B_2''}^{a,a1} = |v_{J_1}\rangle\Gamma_{v,\mathbf{k}_J} - |v_{J_2}\rangle\Gamma_{v,\mathbf{k}_J}$$

$$\propto \hat{z}[\sin(\mathbf{k}_{J_1}\cdot\mathbf{r}) + \sin(\mathbf{k}_{J_2}\cdot\mathbf{r}) + \sin(\mathbf{k}_{J_3}\cdot\mathbf{r})]\Gamma_{v,\mathbf{k}_J},$$

where the $\Gamma_{v,\mathbf{k}_J}$ are equivalent for each element of the $\star\mathbf{k}$ due to the isotropic effective mass of the J-point valence band. A plot of the magnetic field ($\hat{z}$ component) for the symmetry basis modes $\mathbf{B}_{A_2''}^{a,a1}$ and $\mathbf{B}_{B_2''}^{a,a1}$ are given in Figs. 5(a) and 5(b).

2D FDTD simulations of the acceptor-type cavity of Fig. 3(b) and Table I were also performed. The two deepest modes within the first order band gap are found to be of A_2'' and B_2'' symmetry, the same symmetry as the modes predicted by the approximate analysis. Plots of the FDTD calculated magnetic field patterns of these modes are given in Figs. 5(c) and 5(d), again showing a strong resemblance to the approximately generated field patterns. Figures 5(e)–5(h) shows a series of plots of the envelope ($\Gamma_{v,\mathbf{k}_{J_1}}$) of the acceptor mode $\mathbf{B}_{A_2''}^{a,a1}$. The size and shape (isotropic) of the FDTD calculated mode envelope corresponds very nicely with the approximate Wannier envelope as can be seen by the Gaussian fits in Figs. 5(g) and 5(h) and the values of the fit decay constants given in Table III. A similar envelope was extracted for mode $\mathbf{B}_{B_2''}^{a,a1}$, its fit decay constants given in Table III as well.

IV. SUMMARY

A Wannier-like equation for photons in two-dimensional photonic crystal and slab photonic crystal structures is derived. As in the case of electrons in a crystalline material, the curvature of the underlying band structure determines the effective mass of photon wavepackets. A quantitative relation for the effective trapping potential for localized photon states is derived and shown to be proportional to the perturbation of the inverse dielectric constant of the lattice and to its gradient. The Wannier-like equation, with an effective mass tensor determined perturbatively from the Bloch modes at the band extrema, is used to calculate the approximate envelope for localized TE-like modes of a parabolically graded hexagonal photonic crystal defect cavity. The approximate localized modes of both donor-type and acceptor-type defects are considered, using a symmetry analysis to compute the dominant Fourier components of each mode formed by mixing of the degenerate satellite extrema. Numerical finite-difference time-domain calculations of the exact localized modes are also presented. For the cavities considered, a good correspondence between the exact numerical calculations and the solutions to the approximate coupled Wannier-like equations is found.

The Wannier-like equation for the envelope of localized photon states in periodic dielectric structures puts on a more solid foundation the concept of how localized donor and acceptor modes are formed. Specifically, one may predict the symmetry and shape of the envelope of localized states in addition to their dominant Fourier components. More than just building upon one's intuition, this knowledge is of practical importance to the integration and application of photonic crystal devices. As shown for the donor modes of the graded defect within the hexagonal photonic crystal, the highly directed envelope results in an in-plane radiation pattern suited to coupling into external waveguides. In contrast, for the acceptor modes of the hexagonal photonic crystal, the envelope is approximately isotropic resulting in an in-plane radiation pattern much less amenable to waveguide coupling. An understanding of the mode mixing involved in forming localized resonant modes is also of great importance in the design of low-loss waveguides and high-Q resonant cavities

of slab photonic crystals, where coupling to radiation modes of the slab must be minimized.

APPENDIX: ELECTRIC AND MAGNETIC FIELD EIGENOPERATORS

We begin with Maxwell's equations in a (lossless) dielectric medium free of currents and free charge,

$$\begin{aligned}\nabla\times\mathbf{E}&=-i\omega\mathbf{H},\\ \nabla\times\mathbf{H}&=+i\omega(n/c)^2\mathbf{E},\\ \nabla\cdot(n^2\mathbf{E})&=0,\\ \nabla\cdot\mathbf{H}&=0,\end{aligned}\tag{A1}$$

where $\mathbf{E}$ and $\mathbf{H}$ are the harmonic complex electric and magnetic fields, respectively, with time dependence $e^{+i\omega t}$ (the physical fields are found by taking the real part of the complex fields). The velocity of light in vacuum is represented by c, and we have assumed that the material is non-magnetic ($\mu=\mu_o$). We also assume here that the dielectric function does not depend on spatial or temporal frequency, $\epsilon(\omega,\mathbf{k},\mathbf{r})=\epsilon_o n^2(\mathbf{r})$. From the above Maxwell relations, a wave equation for both the electric and magnetic fields can be generated:

$$\eta(\mathbf{r})(\nabla\times\nabla\times\mathbf{E})=\left(\frac{\omega}{c}\right)^2\mathbf{E},\tag{A2}$$

$$\nabla\times(\eta(\mathbf{r})\nabla\times\mathbf{H})=\left(\frac{\omega}{c}\right)^2\mathbf{H},\tag{A3}$$

where $\eta(\mathbf{r})\equiv 1/n^2(\mathbf{r})$.

1. Two-dimensional photonic crystals

In a two-dimensional dielectric structure, or in a dielectric structure in which the refractive index does not vary in a third dimension ($\hat{z}$) orthogonal to the wave vector components of the field, the eigenmodes of Maxwell's equations separate into two classes, transverse electric (TE) and transverse magnetic (TM). As we will be interested in extending our theory to quasi-2D systems consisting of weak vertical waveguides (slab waveguide photonic crystals), we shall use the convention that TE modes are those for which the magnetic field is a scalar field polarized along the $\hat{z}$ direction, and the electric field is polarized in the plane of the 2D PC (*transverse* to the waveguiding direction). Similarly for the TM modes, the electric field is a scalar field polarized along the $\hat{z}$ direction and the magnetic field has only components within the plane of the PC waveguide. For the fundamental vertical waveguide modes of a 2D PC slab waveguide, the modes are only *approximately* TE and TM in nature, the polarization of the fields being exactly TE or TM in nature only in the center of a symmetric slab PC waveguide. For a symmetric slab PC waveguide, the fundamental even modes are TE-like and the fundamental odd modes are TM-like. From here on we make no distinction between the 2D and the quasi-2D systems, realizing that in the case of the quasi-2D PC slab waveguides we have only an approximate theory which neglects polarization mixing and all out-of-plane effects.

We begin with the TE modes in which the magnetic field is described by a scalar field, $\mathbf{H}=\hat{z}H$. As we have assumed that the refractive index does not vary (or the variation can be approximately neglected) in the $\hat{z}$-direction, $\partial_z\eta(\mathbf{r})=0$. The Hermitian eigenvalue equation which results from Eq. (A3) and $\nabla\cdot\mathbf{H}=0$ is (in the 2D case we only consider variations with respect to the in-plane coordinates, $\nabla\equiv\nabla_\perp$)

$$\hat{\mathcal{L}}_H^{\mathrm{TE}}H=\lambda H,\tag{A4}$$

with the TE eigenoperator given by

$$\hat{\mathcal{L}}_H^{\mathrm{TE}}=-(\nabla\eta)\cdot\nabla-\eta\nabla^2.\tag{A5}$$

The eigenvalue, λ, is related to the square of the frequency of the mode, $\lambda=(\omega/c)^2$. As we consider TE-like modes of (quasi-)2D PCs in the body of the text, the eigenoperator $\hat{\mathcal{L}}_H^{\mathrm{TE}}$ and perturbations to it are the main concern of this article.

The situation is slightly more complicated for the TM modes. In this case the electric field is a scalar field, $\mathbf{E}=\hat{z}E$. Unfortunately, the eigenoperator for the electric field is not Hermitian[36] where the standard inner product of fields, $\langle\mathbf{E}|\mathbf{E}\rangle\equiv\int d\mathbf{r}\,\mathbf{E}^*\cdot\mathbf{E}$, is used. As in Refs. 27 and 28, a modified metric which depends upon the dielectric constant may be employed in describing a generalized Hermitian system in terms of the electric field. As an alternative to using the scalar electric field in the case of TM modes, one may consider the vector magnetic field eigenoperator, and corresponding effective Wannier potential, as discussed below in the case of three-dimensional photonic crystals.

2. Three-dimensional photonic crystals

In this case we must use a vector eigenoperator. For reasons discussed above, it is cleaner to consider the magnetic field (divergenceless field with a Hermitian eigenoperator in the case of non-magnetic materials). The vector eigenoperator in the case of a three-dimensional dielectric system is

$$\hat{\boldsymbol{\mathcal{L}}}_H^{3D}=-\eta\nabla^2+(\nabla\eta)\times\nabla\times.\tag{A6}$$

As this operator is linear in η, a perturbation in the dielectric given by $\Delta\eta$ results in the vector perturbation operator

$$\hat{\boldsymbol{\mathcal{L}}}_H'^{,3D}=-\Delta\eta\nabla^2+[\nabla(\Delta\eta)]\times\nabla\times.\tag{A7}$$

The only modification to the effective Wannier equation for a 3D PC is in the effective perturbation potential. Each of the components of the magnetic field are still multiplied by a single envelope function in the 3D PC case, however, the effective Wannier potential is more generally given as

$$\begin{aligned}\Delta\eta_{j,i}'^{,3D,H}(\mathbf{r})=&\,\Delta\eta(\mathbf{r})K_{l,l}^{3D,H}(\mathbf{k}_i,\mathbf{k}_j,\mathbf{G}_{j,i})\\ &+[\nabla(\Delta\eta(\mathbf{r}))]\cdot\mathbf{L}_{l,l}^{3D,H}(\mathbf{k}_i,\mathbf{k}_j,\mathbf{G}_{j,i}),\end{aligned}\tag{A8}$$

$$K^{3D,H}_{l',l}(\mathbf{k}',\mathbf{k},\mathbf{G}) = -\int_v d^3r(\mathbf{h}_{l',\mathbf{k}'})^* \cdot [e^{i\mathbf{G}\cdot\mathbf{r}}(\nabla^2 + 2i\mathbf{k}\cdot\nabla - |\mathbf{k}|^2)]\mathbf{h}_{l,\mathbf{k}} \equiv -\langle \mathbf{h}_{l',\mathbf{k}'}|e^{i\mathbf{G}\cdot\mathbf{r}}(\nabla^2 + 2i\mathbf{k}\cdot\nabla - |\mathbf{k}|^2)|\mathbf{h}_{l,\mathbf{k}}\rangle_v , \quad \text{(A9)}$$

$$\mathbf{L}^{3D,H}_{l',l}(\mathbf{k}',\mathbf{k},\mathbf{G}) = -\int_v d^3r(\mathbf{h}_{l',\mathbf{k}'})^* \times [e^{i\mathbf{G}\cdot\mathbf{r}}(\nabla \times + i\mathbf{k}\times)]\mathbf{h}_{l,\mathbf{k}} \equiv -\langle \mathbf{h}_{l',\mathbf{k}'}|e^{i\mathbf{G}\cdot\mathbf{r}}(\nabla \times + i\mathbf{k}\times)|\mathbf{h}_{l,\mathbf{k}}\rangle'_v . \quad \text{(A10)}$$

*Electronic address: opainter@its.caltech.edu; URL: http://www.its.caltech.edu/~aphhome/painter.html

[1] E. M. Purcell, Phys. Rev. **69**, 681 (1946).
[2] D. Kleppner, Phys. Rev. Lett. **47**, 233 (1981).
[3] E. Yablonovitch, Phys. Rev. Lett. **58**, 2059 (1987).
[4] D. M. Atkin, P. S. J. Russell, T. A. Birks, and P. J. Roberts, J. Mod. Opt. **43**, 1035 (1996).
[5] P. S. J. Russell, D. M. Atkin, and T. A. Birks, *Bound Modes Of Two-Dimensional Photonic Crystal Waveguides* (Kluwer, Dordrecht, 1996), pp. 203–218.
[6] S. G. Johnson, S. Fan, P.R. Villeneuve, J. D. Joannopoulos, and L.A. Kolodziejaki, Phys. Rev. B **60**, 5751 (1999).
[7] J. S. Foresi, P. R. Villeneuve, J. Ferrera, E. R. Thoen, G. Steinmeyer, S. Fan, J. D. Joannopoulos, L. C. Kimerling, H. I. Smith, and E. P. Ippen, Nature (London) **390**, 143 (1997).
[8] O. Painter, J. Vučković, and A. Scherer, J. Opt. Soc. Am. B **16**, 275 (1999).
[9] R. Coccioli, M. Boroditsky, K. W. Kim, Y. Rahmat-Samii, and E. Yablonovitch, IEE Proc.: Optoelectron. **145**, 391 (1998).
[10] O. Painter, R. K. Lee, A. Yariv, A. Scherer, J. D. O'Brien, P. D. Dapkus, and I. Kim, Science **284**, 1819 (1999).
[11] S. Noda, A. Chutinan, and M. Imada, Nature (London) **407**, 608 (2000).
[12] N. Stefanou and A. Modinos, Phys. Rev. B **57**, 12 127 (1998).
[13] A. Yariv, *Optical Electronics*, 4th ed. (Saunders College Publishing, Orlando, FL, 1991).
[14] S. Olivier, C. Smith, M. Rattier, H. Benisty, C. Weisbuch, T. Krauss, R. Houdré, and U. Oesterlé, Opt. Lett. **26**, 1019 (2001).
[15] E. Ozbay, M. Bayindir, I. Bulu, and E. Cubukcu, IEEE J. Quantum Electron. **38**, 837 (2002).
[16] P. S. J. Russell and T. A. Birks, J. Lightwave Technol. **17**, 1982 (1999).
[17] P. S. J. Russell and T. A. Birks, *Bloch Wave Optics in Photonic Crystals: Physics and Applications* (Kluwer, Dordrecht, 1996), pp. 71–91.
[18] G. H. Wannier, Phys. Rev. **52**, 191 (1937).
[19] N. W. Ashcroft and N. D. Mermin, *Solid State Physics* (Saunders College Publishing, New York, 1976).
[20] J. Arnaud, IEE Electron. Lett. **21**, 538 (1985).
[21] J. E. Sipe, L. Poladian, and C. M. de Sterke, J. Opt. Soc. Am. A **11**, 1307 (1994).
[22] C. M. de Sterke, D. J. Salinas, and J. E. Sipe, Phys. Rev. E **54**, 1969 (1996).
[23] J. C. Slater, Phys. Rev. **76**, 1592 (1949).
[24] C. Kittel and A. H. Mitchell, Phys. Rev. **96**, 1488 (1954).
[25] J. M. Luttinger and W. Kohn, Phys. Rev. **97**, 869 (1955).
[26] G. H. Wannier, Rev. Mod. Phys. **34**, 645 (1962).
[27] N. F. Johnson and P. M. Hui, Phys. Rev. B **48**, 10 118 (1993).
[28] M. Charbonneau-Lefort, E. Istrate, M. Allard, J. Poon, and E. H. Sargent, Phys. Rev. B **65**, 125318 (2002).
[29] E. Istrate, M. Charbonneau-Lefort, and E. H. Sargent, Phys. Rev. B **66**, 075121 (2002).
[30] A. Baldereschi, Phys. Rev. B **1**, 4673 (1970).
[31] M. Lončar, T. Doll, J. Vučković, and A. Scherer, J. Lightwave Technol. **18**, 1402 (2000).
[32] P. C. Sercel and K. J. Vahala, Phys. Rev. B **42**, 3690 (1990).
[33] W. Kohn and J. M. Luttinger, Phys. Rev. **98**, 915 (1955).
[34] O. Painter and K. Srinivasan, Phys. Rev. B (unpublished).
[35] M. Tinkham, *Group Theory and Quantum Mechanics*, International Series in Pure and Applied Physics (McGaw-Hill, Inc., New York, 1964).
[36] J. D. Joannopoulos, R. D. Meade, and J. N. Winn, *Photonic Crystals* (Princeton University Press, Princeton, NJ, 1995).
[37] O. Painter, K. Srinivasan, J. D. O'Brien, A. Scherer, and P. D. Dapkus, J. Opt. Soc. Am. A **3**, S161 (2001).
[38] J. E. Sipe, Phys. Rev. E **62**, 5672 (2000).
[39] It should be noted that the envelope is always a scalar field, regardless of the vector nature of the electric or magnetic field.
[40] As discussed in Ref. 38, the $h_{l,\mathbf{k}_o}$ are not complete in the space of lattice periodic functions due to the divergenceless nature of the magnetic field. In order to form a complete basis one must include zero frequency unphysical solutions. As we neglect the contribution of remote bands in our analysis, which the zero frequency solutions certainly are, no significant additional error is to be expected.
[41] We use the term ''mass'' here in analogy to solid-state physics where the curvature of the band structure is related to the inverse of an effective elecron mass. The m^* as defined here is unitless.